

# Impedance Matching and Emission Properties of Nanoantennas in an Optical Nanocircuit

Jer-Shing Huang, Thorsten Feichtner, Paolo Biagioni, and Bert Hecht\*

*Nano-Optics & Biophotonics Group, Department of Experimental Physics 5, Röntgen Research Center for Complex Material Research (RCCM), Physics Institute, University of Würzburg, Am Hubland, D-97074 Würzburg, Germany*

Received December 25, 2008; Revised Manuscript Received March 4, 2009

## ABSTRACT

An experimentally realizable prototype optical nanocircuit consisting of a receiving and an emitting nanoantenna connected by a two-wire optical transmission line is studied using finite-difference time- and frequency-domain simulations. To optimize the coupling between optical nanocircuit elements we apply impedance matching concepts in analogy to radio frequency technology. We show that the degree of impedance matching, and in particular the impedance of the emitting nanoantenna, can be inferred from the experimentally accessible standing wave pattern on the transmission line. We demonstrate the possibility of matching the nanoantenna impedance to the transmission line by variations of the antenna length and width realizable by modern microfabrication techniques. The radiation efficiency of the emitting antenna also depends on its geometry but is independent of the degree of impedance matching. The case study presented here provides the basis for experimental realizations of general optical nanocircuits based on readily available gold nanostructures and a large variety of derived novel devices.

Miniaturization and packaging density of integrated optics based on dielectrics is limited by the wavelength scale modal profiles of guided modes.<sup>1</sup> In contrast, plasmonic modes on noble metal nanostructures offer strong subwavelength confinement and therefore promise the realization of nanometer-scale integrated optical circuitry.<sup>2,3</sup> A truly sub-wavelength integrated optical circuit based on plasmonic nanostructures will generally consist of (i) a set of optical antennas<sup>4-7</sup> to efficiently excite specific local modes by far-field radiation, (ii) a very small footprint network of optical transmission lines<sup>8</sup> (OTLs) to distribute and manipulate plasmonic excitations,<sup>9-16</sup> and (iii) another set of optical antennas to efficiently convert local modes into propagating photons. The properties of metal nanoparticle chains,<sup>17,18</sup> metal nanowires,<sup>19,20</sup> line defects in plasmonic photonic crystals,<sup>21</sup> as well as gaps,<sup>22-24</sup> and v-shaped grooves<sup>9,25,26</sup> in extended metal films have been explored as subwavelength waveguides for light. Efficient launching of specific guided modes on such structures is difficult since it requires matching of both the small mode extension and the k-vector. It has been shown recently that efficient coupling between far-field photons and subwavelength spatial domains can be achieved using resonant optical antennas.<sup>5,7,27-31</sup> However, so far optical antennas have mostly been studied as isolated

elements. Here we consider optical antennas as integral parts of an experimentally realizable integrated optical nanocircuit where they act as efficient interfacing elements between propagating photons and guided modes of a plasmonic two-wire transmission line. We show by simulations that the principles of classical transmission line theory, for example, impedance matching,<sup>32</sup> between the two-wire OTL and dipole antennas are fully applicable at optical frequencies. Impedances of optical circuit elements, in particular impedances of isolated optical antennas, have been introduced before and the possibility of tuning such impedances by optical nanocircuits has been described.<sup>33-36</sup> Here we exploit the fact that the antenna impedance can be tuned by changing the experimentally accessible antenna dimensions. We further show that complex impedances of circuit elements at optical wavelength may be experimentally obtained in terms of reflection coefficients and that impedance matching can be achieved at optical frequencies where connection wires of finite width are used in contrast to well-defined feed points typically encountered in the radio frequency (rf) regime.<sup>34</sup> We finally determine the incoupling efficiency from a receiving antenna into the two-wire transmission line, the radiation efficiency of the emitting optical antenna as well as the overall efficiency of the optical nanocircuit. We would like to point out that because of the plasmonic character of the metals at optical frequencies, which results in a finite penetration depth of light into the metal and a shortened

\* To whom correspondence should be addressed: hecht@physik.uni-wuerzburg.de.

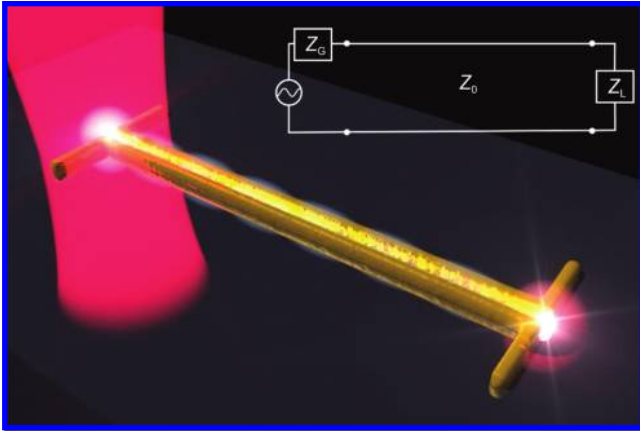


**Figure 1.** Artists view of the overall geometry of an optical nanocircuit consisting of a receiving antenna (left) and a two-wire optical transmission line as well as an emitting antenna. The receiving antenna is excited by a linearly polarized Gaussian source and launches guided modes which propagate along the nanosize two-wire optical transmission line. The emitting antenna (right) converts guided modes into propagating photons. The inset shows the corresponding equivalent circuit consisting of a generator, a transmission line, and a load.

effective wavelength of surface waves, the results obtained here cannot be derived by a simple scaling down of similar systems used at longer wavelengths, where metals behave as ideal conductors.

The system simulated by the finite-difference time-domain method (FDTD Solutions, version 5.1.2, Lumerical Solutions Inc., Vancouver, Canada) contains two dipole nanoantennas connected by a nanosize two-wire OTL with a  $30 \times 30 \text{ nm}^2$  quadratic wire cross section and a wire separation of 10 nm equal to the feed-gap width of both antennas (see Figure 1). The structure is made of gold ( $\epsilon = -26.57 + 1.66j$ )<sup>37</sup> and situated in air ( $\epsilon = 1$ ) on top of a glass half-space ( $\epsilon = 2.11$ ). One of the antennas (left side, receiving antenna) is illuminated by a tightly focused Gaussian beam (spot size = 340 nm,  $\lambda = 830 \text{ nm}$ ) from within the glass half-space with polarization parallel to the antenna. Enhanced and confined optical fields created in the antenna feed-gap are efficiently converted into guided quasi-transverse electric (TE) modes propagating along the transmission line, which are finally converted into far-field photons by the second antenna (emitting antenna). The equivalent circuit of the system is shown in the inset of Figure 1. It consists of a generator providing an ac-voltage at the chosen optical frequency including the generator impedance  $Z_G$  representing the receiving antenna, a transmission line with characteristic impedance  $Z_0$ , as well as a load impedance  $Z_L$  representing the emitting antenna. In the following we show that the coupling efficiency between elements of this prototype optical nanocircuit is governed by the degree of impedance matching. We also outline how impedance matching can be achieved by variation of experimentally accessible geometrical parameters.

As a first step we optimize the coupling of the receiving antenna to an infinitely long OTL, which is characterized by its characteristic impedance,  $Z_0$ .<sup>32</sup> To mimic an infinitely long transmission line in the simulation, the OTL extends

long enough ( $>3000 \text{ nm}$ ) inside the simulation area before being terminated by the perfectly matched layer boundary. Because of the considerable damping of the guided modes on the OTL the amplitude of reflected fields reaching the receiving antenna is negligible, as required for a system of infinite length. To optimize the coupling of far-field power into the OTL guided modes we vary the length of the receiving antenna (cross section  $30 \times 30 \text{ nm}^2$ ) and record the intensity enhancement in the antenna feed-gap (point P) and at an equivalent position at a distance of 1000 nm down the OTL (point Q). The results are plotted in Figure 2a along with the intensity enhancement obtained in the feed-gap of an isolated dipole antenna of the same geometry. Compared to the isolated dipole antenna, the OTL-connected antenna shows a lower intensity enhancement but exhibits a resonance at about the same total length of 200 nm, which is kept constant in all further simulations. We tentatively conclude that attaching a two-wire OTL oriented perpendicular to the electric fields in the feed-gap does not significantly affect the antenna resonance length. It is also evident that the maxima of the intensity enhancements at point P and Q coincide. This implies that the antenna resonance and the coupling efficiency into the waveguide for the chosen geometry can be optimized for the same antenna length. Compared to the same transmission line without receiving antenna, the far-field power coupling improves by more than a factor of 200 with a resonant receiving antenna.

Having efficiently launched guided modes on the OTL we are interested in their propagation constants.<sup>32</sup> Figure 2b shows the intensity enhancement along a line marking the center of the transmission line (red cross in the inset), while Figure 2c shows the intensity enhancement in a plane 15 nm above and parallel to the glass/air interface (red dotted line in the inset). A strong exponential damping of the intensity enhancement is observed with superimposed slow undulations close to the receiving antenna. The slow undulations are due to the beating of at least three modes with different propagation constants (Supporting Information, Figure S1). After a distance of 500 nm from the receiving antenna these undulations cease and only the fundamental mode prevails. A very small modulation is observed close to the end of the simulation area due to a weak reflection from the perfectly matched layer boundary. Exploiting this modulation and the overall exponential decay we determine the complex propagation constant of the guided fundamental TE mode  $\gamma = (0.00084 + 0.02802j) \text{ nm}^{-1}$  by nonlinear fitting of the curve in Figure 2b. From this we obtain a decay length of 1190 nm and an effective wavelength of 224 nm, which is much shorter than the free-space wavelength.<sup>38,39</sup> An independent simulation using the full-vectorial finite-difference frequency-domain (FDFD) method<sup>40</sup> (MODE Solutions, version 3.0.1, Lumerical Solutions Inc., Vancouver, Canada) yields similar results. The propagation constants of the two higher-order modes (one very short-ranged, one longer-ranged but very low intensity) are determined by a stepwise fitting of respective segments of the decay (Supporting Information, Figure S1). The inset of Figure 2b shows the near-field intensity modal profile of the fundamental

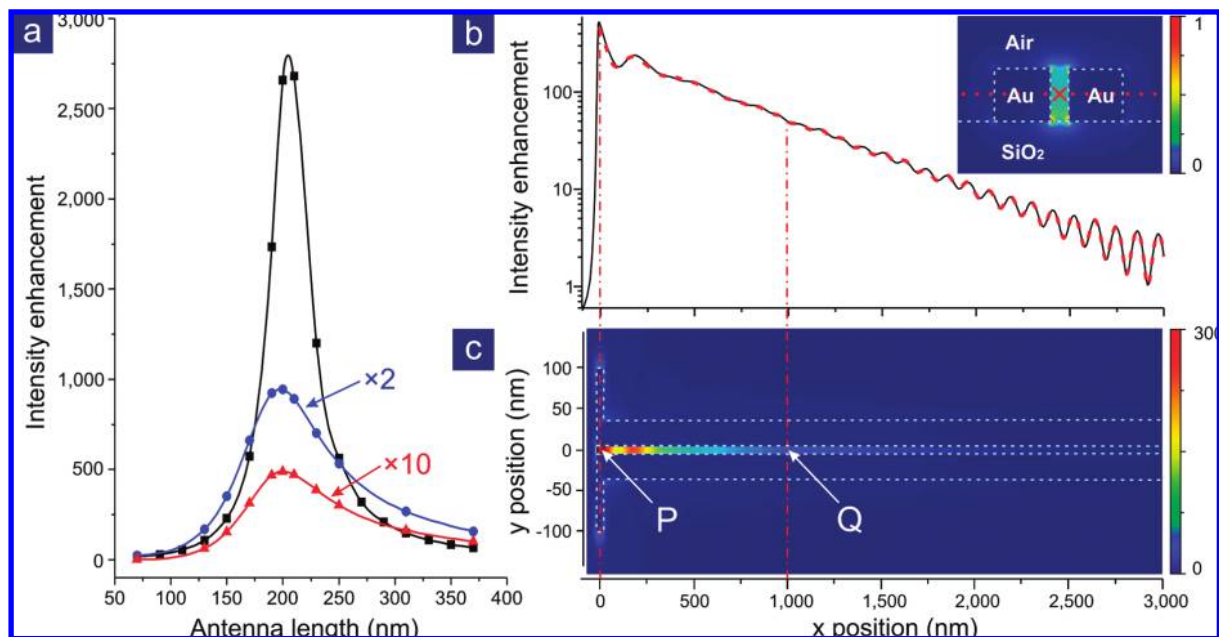


**Figure 2.** Receiving antenna and infinitely long optical transmission line. (a) Intensity enhancement in the feed-gap as a function of the total antenna length for an isolated dipole antenna (black squares), the gap of an antenna connecting to the optical transmission line (multiplication factor,  $\times 2$ ; blue dots), as well as the field enhancement along the center of the transmission line (multiplication factor,  $\times 10$ ; red triangles). (b) Line cut of the intensity enhancement along the center of the transmission line. Red dashed line shows the best fit. The inset shows the normalized modal intensity profile of the fundamental guided TE mode. (c) 2D map of the intensity enhancement recorded in a plane parallel to the substrate, 15 nm above the glass/air interface, indicated by the red dotted line in the inset of panel b. Note the unequal scales in  $x$  and  $y$  directions.

mode. The corresponding distributions of the electric ( $\mathbf{E}$ ) and magnetic ( $\mathbf{H}$ ) field components are plotted in the Supporting Information, Figure S2. The characteristic impedance of the two-wire OTL is defined as  $Z_0 = V/I$ . The voltage  $V$  between two finite-width wires is obtained by a line integral over the complex electric field  $\mathbf{E}$  from one wire core to the other, as indicated by the red-dashed line in Figure S2, Supporting Information, while the current  $I$  is evaluated based on Ampère's law. Since the magnetic field  $\mathbf{H}$  is zero at infinity, we replace the typical close-loop integration path with a sufficiently long path approximating a linear path from  $y = -\infty$  to  $y = +\infty$ . The OTL characteristic impedance thus obtained has a value of  $Z_0 = (216 - 5.5j) \Omega$ , which is comparable to impedances of two-wire transmission lines at radio frequencies.<sup>32</sup> The robustness of this method is confirmed by the very weak dependence of  $Z_0$  on the choice of the integration path ( $\Delta Z_0 < 6\%$ ), which is due to the weak inhomogeneity of the field distribution inside the gap.

Knowing the complex propagation constant of the fundamental TE mode supported by the two-wire OTL and its characteristic impedance we are able to quantitatively study effects that occur in optical nanocircuits based on finite-length OTLs. In Figure 3, we compare a finite-length open OTL ( $L = 1344$  nm, Figure 3a) with the same OTL terminated by an emitting antenna serving as an arbitrary load (Figure 3b). Corresponding 2D images of the intensity enhancement recorded in the same plane as Figure 1c are shown in the lower panel of Figure 3. Owing to a finite impedance mismatch between the OTL and the load we observe characteristic standing wave patterns. The complex voltage reflection coefficient  $\Gamma_V$  for the discontinuity can be

determined by nonlinear fitting of these standing wave patterns between the centers of two antennas. As to be expected from classical transmission line theory, the open end termination of the OTL leads to a near 100% reflectivity ( $|\Gamma_V| = 95.6\%$ ) while the termination with the particular antenna of Figure 3b results in a much lower reflectivity ( $|\Gamma_V| = 37.3\%$ ). The deviation from perfect reflection of the open-ended OTL is due to residual radiation from the truncated finite-width nanowires.

Since the reflectivity is a direct measure of the impedance matching between the OTL and the load, the load impedance  $Z_L$  can be determined according to

$$Z_L = Z_0 \frac{1 + \Gamma_V}{1 - \Gamma_V} \quad (1)$$

once the complex reflection coefficient is known.<sup>32</sup> This approach avoids ambiguities that occur due to the fact that at optical frequencies, as opposed to the radiowave and microwave regime, the finite extension of nanostructures in the optical nanocircuit can no longer be neglected since the fields vary strongly over the emitting antenna's gap volume (see for example Figure 3b). Therefore, the concept of a feed "point" is difficult to apply, which makes it impractical to evaluate impedances by calculating the voltage to current ratio. From an experimental point of view, since plasmon propagation and standing waves on the OTL can be observed experimentally, for example, by photoemission electron microscopy<sup>41,42</sup> or scanning near-field optical microscopy,<sup>43,44</sup> it is possible to use this approach to determine impedances of circuit elements at optical frequencies.

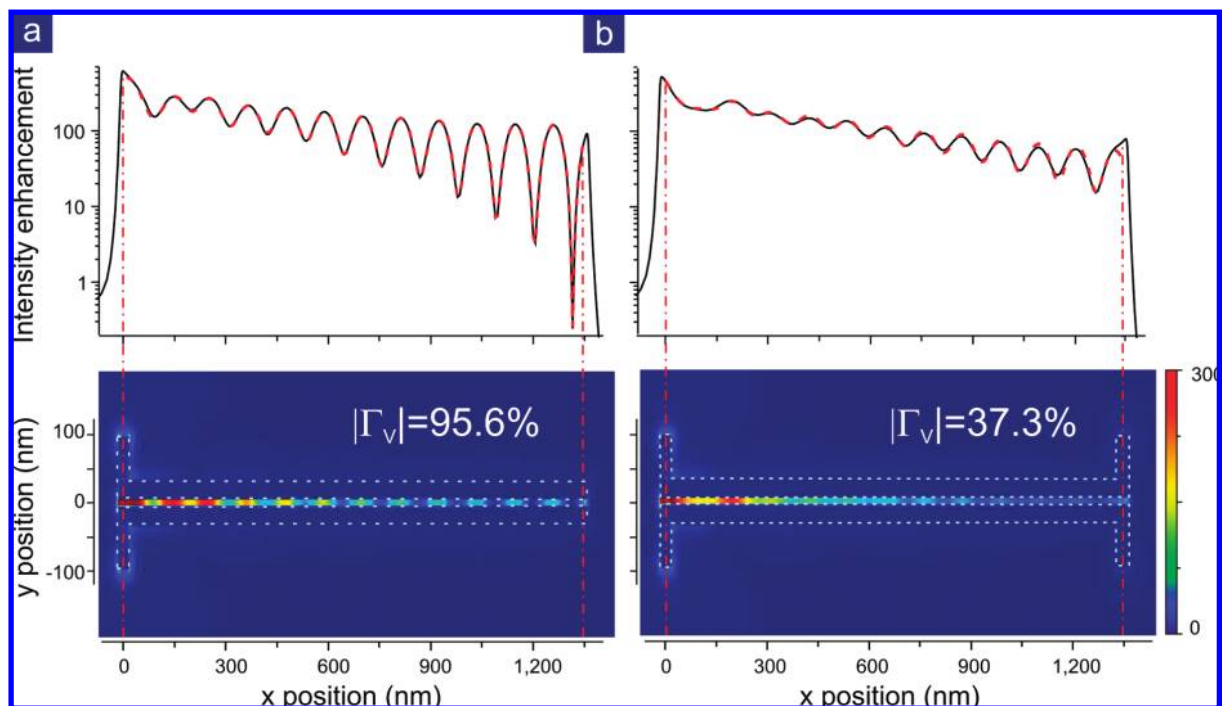


**Figure 3.** Effect of different loads on reflectivity. Upper panels: Line cut and best fit (red dashed line) of the intensity enhancement in the gap of a 1344 nm long optical transmission line terminated by (a) an open end (equivalent to antenna length 70 nm) and (b) a 200 nm long emitting antenna. Lower panels: corresponding 2D field enhancement maps. The respective voltage reflectivities at the terminations are indicated. Note the unequal scales in  $x$  and  $y$  directions.

To minimize the voltage reflection coefficient at the load antenna, we scan the length and the width of the emitting antenna to achieve optimal impedance matching. While the effects of scanning the antenna length can be understood in analogy to classical antenna theory, we assume that by changing the antenna width we change the effective wavelength of the plasmonic mode on the nanowire.<sup>38</sup> Figure 4a shows the voltage reflectivity [ $|\Gamma_V| = (\Gamma_V \Gamma_V^*)^{1/2}$ ] as a function of the total length of the emitting antenna varied between 70 and 610 nm. Plotted in different colors are traces obtained for antennas with widths of 30, 40, 50, and 60 nm, while the structure height is always kept constant at 30 nm. All plots clearly show two distinct minima, which can be related to the respective best matching of the antenna impedance to  $Z_0$  for a given width. Using eq 1, the input impedances of the respective emitting antennas can be calculated. The results are plotted in Figure 4b. For a fixed antenna width, the antenna impedance describes a spiral in the complex impedance plane where the position of  $Z_0$  is also marked. We observe that as the antenna width is increased the average radius of the impedance spirals decreases while simultaneously the spirals shift to smaller resistances. This behavior is in full analogy to that of radiowave antennas.<sup>45</sup> A shorter distance  $|Z_L - Z_0|$  in the complex  $Z_L$  plane indicates better impedance matching. The shortest distance  $|Z_L - Z_0|$  on the plane (Figure 4b) obtained for a 610 nm long and 50 nm wide antenna corresponds to the minimum reflectivity ( $|\Gamma_V| = 2.7\%$ ) in Figure 4a.

We note that there are other parameters, apart from the antenna width, that one may change to optimize the imped-

ance matching between two-wire OTL and antenna, for example, the widths of the OTL's wires and the gap between them, as well as the connection geometry.<sup>45</sup> Furthermore, the analogy to classical transmission line theory suggests that passive elements such as "stubs" may be used in passive impedance matching circuits<sup>32</sup> at optical frequencies.

Having optimized the impedance matching between the OTL and the emitting antenna, we are interested in the radiation efficiency of the emitting antenna as well as in the overall power transmission of the circuit. So far we have shown that by changing structural dimensions of the involved circuit elements, impedance matching can be achieved and  $|\Gamma_V|$  can be minimized. The minimum  $|\Gamma_V|$ , however, only results in the maximum transportation of power if  $Z_0$  is real. Since  $Z_0$  is complex in our work, the time-averaged power delivered to the load is not given by the difference between the powers of the incident and reflected wave.<sup>46</sup> We therefore employ the concept of power waves and Kurokawa's method<sup>47</sup> to describe the power flow in the optical nanocircuit. Using the concept of power waves, the power reflection coefficient  $\Gamma_P$  can be expressed as

$$\Gamma_P = \left| \frac{Z_L - Z_0^*}{Z_L + Z_0} \right|^2 \quad (2)$$

where  $Z_0$  represents the impedance seen by the emitting antenna (load).  $\Gamma_P$  calculated according to eq 2 is plotted in Figure 5a while an equivalent Smith chart, mapping the modified impedance as mentioned by Kurokawa<sup>45</sup> and used

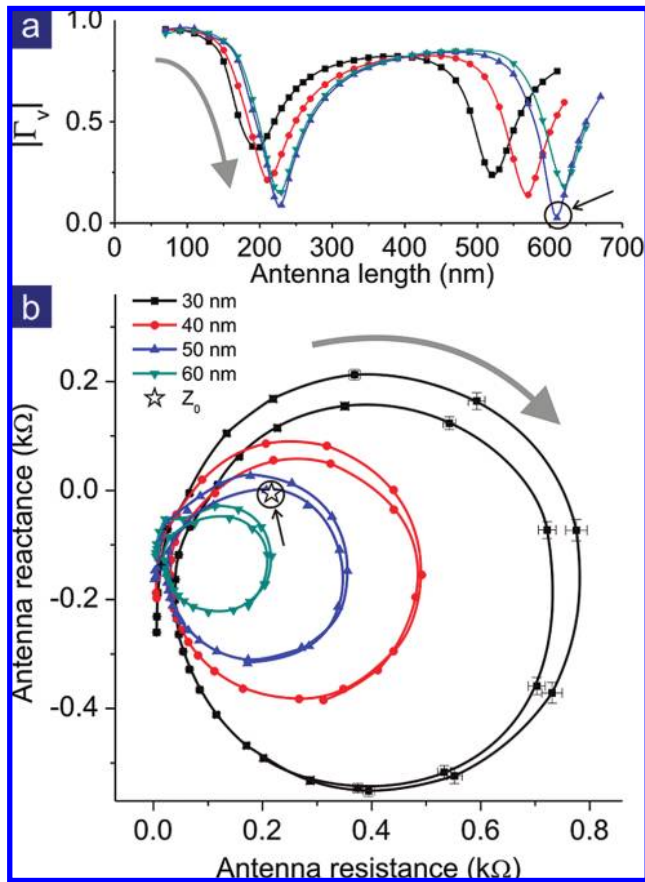


**Figure 4.** Emitting antenna: voltage reflectivity and antenna impedance. (a) Voltage reflectivity as a function of emitting antenna's total length for antenna widths of 30 (black), 40 (red), 50 (blue), and 60 nm (green). (b) Input impedance of the emitting antenna in the complex  $Z_L$  plane. Representative error bars resulting from uncertainties of the reflectivity's amplitude and phase are displayed for the 30 nm wide antenna. The open star represents the position of  $Z_0$ . Black arrows and circles denote the point of best impedance matching corresponding to the closest approach of antenna impedance and  $Z_0$ . The gray arrows indicate the direction of increasing total antenna length.

in passive RFID design,<sup>48</sup> is presented in the Supporting Information, Figure S3.

Compared to the voltage reflection coefficient  $\Gamma_V$  in Figure 4a,  $\Gamma_P$  shows a similar trend with small deviations due to the small imaginary part of  $Z_0$ . For the design of structures with high power transmission efficiency, the modified Smith chart (Supporting Information, Figure S3) provides a quick guideline by considering the distance of the respective load impedance to the chart center, which is a direct measure of  $\Gamma_P$ . Since  $\Gamma_P$  describes the power reflection, a minimal  $\Gamma_P$  should result in a maximum power input to the respective emitting antenna. We determine the net time-averaged power flow  $P_{in}$  along the OTL, 95 nm in front of the emitting antenna, by integrating the Poynting vector over a respective plane perpendicular to the OTL, and normalize it with the injected source power  $P_{source}$ . As shown in Figure 5b, the maxima of  $P_{in}/P_{source}$  coincide with the minima of the power reflection coefficient. To evaluate the radiation efficiency of the emitting antenna, we obtain the power  $P_{out}$  radiated from the emitting antenna by integrating the outward Poynting

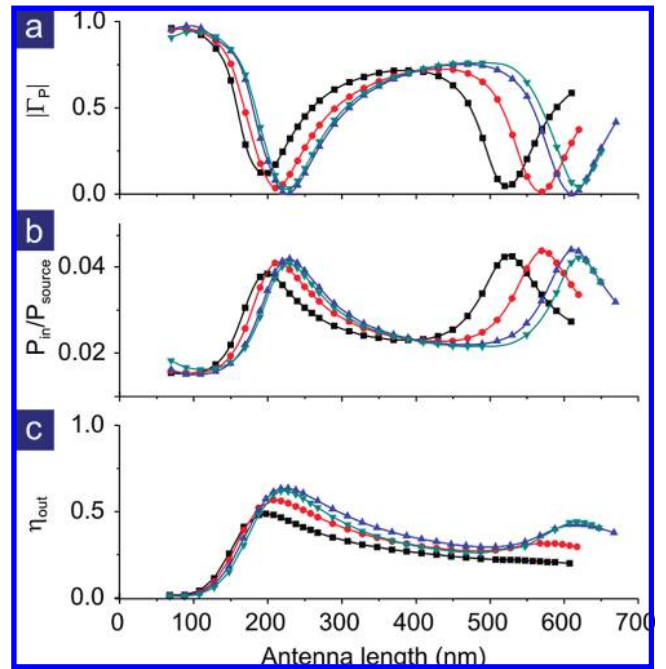


**Figure 5.** Emitting antenna: power delivered and radiation efficiency. (a) Power reflection coefficient as a function of the antenna length for antenna widths of 30 (black), 40 (red), 50 (blue), and 60 nm (green). (b) Input power and (c) radiation efficiency of the emitting antenna, respectively, for the corresponding antenna dimensions. The nonzero offset of  $P_{in}$  is due to the finite radiation of the open-ended OTL and losses in the material.

vector over a closed box that encloses the emitting antenna but excludes a small rectangular area where the transmission line enters the box. We calculate the radiation efficiency  $\eta_{out}$  of the emitting antenna as<sup>45</sup>

$$\eta_{out} = \frac{P_{out}}{P_{in}}. \quad (3)$$

Figure 5c shows the radiation efficiency as a function of the total antenna length for antenna widths varying from 30 to 60 nm. For all antennas the radiation efficiencies increase markedly from close to 0 to about 60% when the antenna length is increased to 200 nm. The first maxima of the radiation efficiency curves seem to coincide with the first minima of the reflectivity curves in Figure 5a, which is a behavior not observed for the second reflectivity minima. Indeed, we find that the concomitance of best conditions for load impedance matching and for maximum radiation efficiency for the first reflectivity minimum is a coincidence. As may be inferred from the deviations between reflectivity minima and radiation efficiency maxima for the second resonances there is in general no reason why an antenna that provides good impedance matching should also provide high radiation efficiency.

To estimate the overall performance of the optical nanocircuit, we finally consider the power flow through the system for the case of best matching, that is, for a 230 nm long and 50 nm wide emitting antenna. The time-averaged power radiated from the emitting antenna  $P_{out}$  can be expressed in terms of the time-averaged Gaussian source power  $P_{source}$  as

$$P_{\text{out}} = \eta_{\text{tot}} P_{\text{source}} = \eta_{\text{out}} (1 - \Gamma_p) e^{-2\alpha L} \eta_{\text{in}} P_{\text{source}} \quad (4)$$

where  $\eta_{\text{tot}}$  is the total efficiency and  $\eta_{\text{in}}$  is the ratio between the time-averaged power coupled into the OTL by the receiving antenna and the source power  $P_{\text{source}}$ . The factors  $(1 - \Gamma_p)$  and  $e^{-2\alpha L}$ , respectively, take into account the power reflection at the emitting antenna and losses along the OTL. We obtain a total efficiency  $\eta_{\text{tot}} = 2.65\%$  and an efficiency of the receiving antenna  $\eta_{\text{in}} = 27.6\%$ . The fairly large value for  $\eta_{\text{in}}$  provides quantitative evidence that the receiving antenna is an efficient collector of far-field radiation, while the much lower value for the overall efficiency  $\eta_{\text{tot}}$  is dominated by propagation losses.

In conclusion, we have proposed and analyzed an experimentally realizable prototype optical nanocircuit consisting of a receiving and an emitting optical antenna connected by a nanosize two-wire OTL. By evaluating standing wave patterns we are able to investigate impedance matching and absolute impedances of circuit elements at optical frequencies. We also point out that a well-matched antenna does not necessarily have the highest radiation efficiency. The evaluation of standing wave patterns should be applicable in practical realizations of optical nanocircuits to experimentally determine impedances of optical nanocircuit elements. Finally, we analyze the power flow and give a quantitative estimation of the relevant efficiencies for power transfer in the system. Our work clearly shows that systems of interconnected nano-optical elements can be optimized by applying concepts of impedance matching which may also be applied to understand and control the coupling between single quantum emitters and metallic nanostructures.

**Acknowledgment.** The authors thank D. W. Pohl, L. Su, C. S. Huang, C. Capsoni, M. D'Amico, G. Gentili, and J. Kern for useful scientific discussions. P. Biagioni acknowledges a Humboldt Research Fellowship for Postdoctoral Researcher.

**Note Added after ASAP Publication:** This article was published ASAP on April 1, 2009. Modifications have been made to equation 3. The correct version was published on April 17, 2009.

**Supporting Information Available:** Determination of the propagation constants of TE guided modes and voltage reflectivity; evaluation of OTL characteristic impedance; Smith chart for power wave and power reflection. This material is available free of charge via the Internet at <http://pubs.acs.org>.

## References

- (1) Yariv, A. *Optical Electronics in Modern Communications*; Oxford University Press: Oxford, 1997.
- (2) Barnes, W. L.; Dereux, A.; Ebbesen, T. W. *Nature (London)* **2003**, *424*, 824–830.
- (3) Ozbay, E. *Science* **2006**, *311*, 189–193.
- (4) Pohl, D. W. Near field Optics Seen As an Antenna Problem in near Field Optics: Principles and Applications. *The Second Asia-Pacific Workshop on near Field Optics*; World Scientific: Singapore, 2000.
- (5) Greffet, J.-J. *Science* **2005**, *308*, 1561–1563.
- (6) Schuck, P. J.; Fromm, D. P.; Sundaramurthy, A.; Kino, G. S.; Moerner, W. E. *Phys. Rev. Lett.* **2005**, *94*, 017402.
- (7) Mühlischlegel, P.; Eisler, H.-J.; Martin, O. J. F.; Hecht, B.; Pohl, D. W. *Science* **2005**, *308*, 1607–1609.

- (8) Takahara, J.; Yamagishi, S.; Taki, H.; Morimoto, A.; Kobayashi, T. *Opt. Lett.* **1997**, *22*, 475–477.
- (9) Bozhevolnyi, S. I.; Volkov, V. S.; Devaux, E.; Laluet, J.-Y.; Ebbesen, T. W. *Nature (London)* **2006**, *440*, 508–511.
- (10) Chang, D. E.; Sørensen, A. S.; Demler, E. A.; Lukin, M. D. *Nat. Phys.* **2007**, *3*, 807–812.
- (11) Sukharev, M.; Sideman, T. J. *Chem. Phys.* **2006**, *124*, 144707.
- (12) Aeschlimann, M.; Bauer, M.; Bayer, D.; Brixner, T.; García de Abajo, F. J.; Pfeiffer, W.; Rohmer, M.; Spindler, C.; Steeb, F. *Nature (London)* **2007**, *446*, 301–304.
- (13) Dickson, W.; Wurtz, G. A.; Evans, P. R.; Pollard, R. J.; Zayats, A. V. *Nano Lett.* **2008**, *8*, 281–286.
- (14) Smolyaninov, I. I.; Davis, C. C.; Zayats, A. V. *Appl. Phys. Lett.* **2002**, *81*, 3314–3316.
- (15) Feigenbaum, E.; Orenstein, M. *Opt. Express* **2007**, *15*, 17948–17953.
- (16) Pacifici, D.; Lezec, H. J.; Atwater, H. A. *Nat. Photonics* **2007**, *1*, 402–406.
- (17) Maier, S. A.; Kik, P. G.; Atwater, H. A.; Meltzer, S.; Harel, E.; Koel, B. E.; Requicha, A. A. G. *Nat. Mater.* **2003**, *2*, 229–232.
- (18) Krenn, J. R.; Dereux, A.; Weeber, J. C.; Bourillot, E.; Lacroute, Y.; Goudonnet, J. P.; Schider, G.; Gotschy, W.; Leitner, A.; Aussenegg, F. R.; Girard, C. *Phys. Rev. Lett.* **1999**, *82*, 2590–2593.
- (19) Krenn, J. R.; Weber, J.-C. *J. C. Phil. Trans. R. Soc. London A* **2004**, *362*, 739–756.
- (20) Ditlbacher, H.; Hohenau, A.; Wagner, D.; Kreibig, U.; Rogers, M.; Hofer, F.; Aussenegg, F. R.; Krenn, J. R. *Phys. Rev. Lett.* **2005**, *95*, 257403.
- (21) Bozhevolnyi, S. I.; Erland, J.; Leosson, K.; Skovgaard, P. M. W.; Hvam, J. M. *Phys. Rev. Lett.* **2001**, *86*, 3008–3011.
- (22) Tanaka, K.; Tanaka, M. *Appl. Phys. Lett.* **2003**, *82*, 1158–1160.
- (23) Liu, L.; Han, H.; He, S. *Opt. Express* **2005**, *13*, 6645–6650.
- (24) Lee, I.; Jung, J.; Park, J.; Kim, H.; Lee, B. *Opt. Express* **2007**, *15*, 16596–16603.
- (25) Bozhevolnyi, S. I.; Volkov, V. S.; Devaux, E.; Ebbesen, T. W. *Phys. Rev. Lett.* **2005**, *95*, 046802.
- (26) Volkov, V. S.; Bozhevolnyi, S. I.; Devaux, E.; Laluet, J.-Y.; Ebbesen, T. W. *Nano Lett.* **2007**, *7*, 880–884.
- (27) Farahani, J. N.; Pohl, D. W.; Eisler, H.-J.; Hecht, B. *Phys. Rev. Lett.* **2005**, *95*, 017402.
- (28) Kühn, S.; Hakanson, U.; Rogobete, L.; Sandoghdar, V. *Phys. Rev. Lett.* **2006**, *97*, 017402.
- (29) Kim, S.; Jin, J.; Kim, Y.-J.; Park, I.-Y.; Kim, Y.; Kim, S.-W. *Nature (London)* **2008**, *453*, 757–760.
- (30) Ghenuche, P.; Cherukulappurath, S.; Taminiau, T. H.; van Hulst, N. F.; Quidant, R. *Phys. Rev. Lett.* **2008**, *101*, 116805.
- (31) Anger, P.; Bharadwaj, P.; Novotny, L. *Phys. Rev. Lett.* **2006**, *96*, 113002.
- (32) Cheng, D. K. *Field and Wave Electromagnetics*; Addison Wesley: New York, 1983.
- (33) Engheta, N.; Salandrino, A.; Alù, A. *Phys. Rev. Lett.* **2005**, *95*, 095504.
- (34) Alù, A.; Engheta, N. *Phys. Rev. Lett.* **2008**, *101*, 043901.
- (35) Alù, A.; Engheta, N. *Nat. Photonics* **2008**, *2*, 307–310.
- (36) Alù, A.; Engheta, N. *Phys. Rev. B* **2008**, *78*, 195111.
- (37) Johnson, P. B.; Christy, R. W. *Phys. Rev. B* **1972**, *6*, 4370–4379.
- (38) Novotny, L. *Phys. Rev. Lett.* **2007**, *98*, 266802.
- (39) Barnard, E. S.; White, J. S.; Chandran, A.; Brongersma, M. L. *Opt. Express* **2008**, *16*, 16529–16537.
- (40) Zhu, Z.; Brown, T. G. *Opt. Express* **2002**, *10*, 853–864.
- (41) Cinchetti, M.; Gloskovskii, A.; Nepjiko, S. A.; Schonhense, G.; Rochholz, H.; Kreiter, M. *Phys. Rev. Lett.* **2005**, *95*, 047601.
- (42) Douillard, L.; Charra, F.; Korczak, Z.; Bachelot, R.; Kostcheev, S.; Lerondel, G.; Adam, P.-M.; Royer, P. *Nano Lett.* **2008**, *8*, 935–940.
- (43) Weeber, J.-C.; Krenn, J. R.; Dereux, A.; Lamprecht, B.; Lacroute, Y.; Goudonnet, J. P. *Phys. Rev. B* **2001**, *64*, 045411.
- (44) Zentgraf, T.; Dorfmueller, J.; Rockstuhl, C.; Etrich, C.; Vogelgesang, R.; Kern, K.; Pertsch, T.; Lederer, F.; Giessen, H. *Opt. Lett.* **2008**, *33*, 848–850.
- (45) Lee, K. F. *Principles of Antenna theory*; John Wiley & Sons, New York, 1984.
- (46) Rahola, J. *IEEE Trans. Circuits Syst. II: Express Briefs* **2008**, *55*, 92–96.
- (47) Kurokawa, K. *IEEE Trans. Microwave Theory Tech.* **1965**, *13*, 194–202.
- (48) Nikitin, P. V.; Rao, K. V. S.; Lam, S. F.; Pillai, V.; Martinez, R.; Heinrich, H. *IEEE Trans. Microwave Theory Tech.* **2005**, *53*, 2721–2725.

NL803902T